Earth's Future

RESEARCH ARTICLE
10.1029/2023EF004233

Aggressive Aerosol Mitigation Policies Reduce Chances of Keeping Global Warming to Below 2C

R. Wood[1], M. A. Vogt[1], and I. L. McCoy[2,3,4]

[1]Department of Atmospheric Sciences, University of Washington, Seattle, WA, USA, [2]Cooperative Institute for Research in Environmental Sciences, University of Colorado, Boulder, CO, USA, [3]Chemical Sciences Laboratory, National Oceanic and Atmospheric Administration, Boulder, CO, USA, [4]Cooperative Programs for the Advancement of Earth System Science, University Corporation for Atmospheric Research, Boulder, CO, USA

Key Points:

- Aerosol forcing changes are isolated from CMIP6 projected scenarios using an approximate partial radiative perturbation method
- Aerosol-cloud interactions dominate future aerosol forcing changes from cleanup policies over the period 2020–2050
- Likelihood of maintaining global warming to below 2C will be strongly reduced by implementing aggressive near-term aerosol cleanup policies

Supporting Information:

Supporting Information may be found in the online version of this article.

Correspondence to:

R. Wood,
robwood2@uw.edu

Citation:

Wood, R., Vogt, M. A., & McCoy, I. L. (2024). Aggressive aerosol mitigation policies reduce chances of keeping global warming to below 2C. *Earth's Future*, *12*, e2023EF004233. https://doi.org/10.1029/2023EF004233

Received 31 OCT 2023
Accepted 30 APR 2024
Corrected 22 AUG 2024

This article was corrected on 22 AUG 2024. See the end of the full text for details.

Author Contributions:

Conceptualization: R. Wood, M. A. Vogt, I. L. McCoy
Data curation: M. A. Vogt, I. L. McCoy
Formal analysis: M. A. Vogt, I. L. McCoy
Funding acquisition: R. Wood, I. L. McCoy
Investigation: R. Wood, M. A. Vogt, I. L. McCoy
Methodology: R. Wood, M. A. Vogt, I. L. McCoy
Project administration: R. Wood, I. L. McCoy

Abstract Aerosol increases over the 20th century delayed the rate at which Earth warmed as a result of increases in greenhouse gases (GHGs). Aggressive aerosol mitigation policies arrested aerosol radiative forcing from ∼1980 to ∼2010. Recent evidence supports decreases in forcing magnitude since then. Using the approximate partial radiative perturbation (APRP) method, future shortwave aerosol effective radiative forcing changes are isolated from other shortwave changes in an 18-member ensemble of ScenarioMIP projections from phase 6 of the Coupled Model Intercomparison Project (CMIP6). APRP-derived near-term (2020–2050) aerosol forcing trends are correlated with published model emulation values but are 30%–50% weaker. Differences are likely explained by location shifts of aerosol-impacting emissions and their resultant influences on susceptible clouds. Despite weaker changes, implementation of aggressive aerosol cleanup policies will have a major impact on global warming rates over 2020–2050. APRP-derived aerosol radiative forcings are used together with a forcing and impulse response model to estimate global temperature trends. Strong mitigation of GHGs, as in SSP1-2.6, likely prevents warming exceeding 2C since preindustrial but the strong aerosol cleanup in this scenario increases the probability of exceeding 2C by 2050 from near zero without aerosol changes to 6% with cleanup. When the same aerosol forcing is applied to a more likely GHG forcing scenario (i.e., SSP2-4.5), aggressive aerosol cleanup more than doubles the probability of reaching 2C by 2050 from 30% to 80%. It is thus critical to quantify and simulate the impacts of changes in aerosol radiative forcing over the next few decades.

Plain Language Summary Over the 20th century, fossil fuel burning led to increased concentrations of greenhouse gases (GHGs) and small particles known as aerosols. Aerosols scatter sunlight back to space and enhance cloud brightness and longevity, thus cooling Earth. The amount of warming since the pre-industrial depends upon both GHGs and aerosol. After ∼1980, air quality improvements led to a reduction in this cooling effect, unmasking some of the GHG potential to warm the planet. This has reinforced the importance of understanding the interplay between aerosols and GHGs in climate projections. To examine this sensitivity, we use a set of global climate model simulations forced by a variety of future GHG and aerosol concentration based on plausible socioeconomic pathways. Shifts in the location of regional aerosol emissions has an impact on the global climate, influencing the accuracy of our predictions for Earth's future warming as measured by the probability of increasing global temperatures by 2C by 2050 compared to pre-industrial. Under plausible GHG scenarios, aggressive aerosol cleanup policies can more than double the probability of crossing this threshold. This emphasizes the urgency of improving our simulations in order to accurately predict and quantify the impact of aerosols over the next few decades.

1. Introduction

The increase of atmospheric aerosol loading over the 20th century delayed the rate at which Earth's global mean temperature increased due to increases in well-mixed greenhouse gases (Meehl et al., 2004). The magnitude of present day aerosol forcing remains uncertain (Bellouin et al., 2020). Existing studies have determined and documented aerosol forcing over the historical record with dedicated simulations using climate models (Quaas et al., 2009). Observational studies using satellites also generally support the notion that aerosol forcing may be masking a significant fraction of the greenhouse warming (Bellouin et al., 2020). Aerosol loading globally reached a peak close to the turn of the 21st century (Quaas et al., 2022) due to air quality cleanup policies designed to mitigate the deleterious health impacts of particulate matter, which represent a major global burden of disease (Murray et al., 2020). Anthropogenic aerosol forcing associated with increased aerosol loading arises from

Resources: R. Wood
Software: M. A. Vogt
Supervision: R. Wood, I. L. McCoy
Visualization: M. A. Vogt
Writing – original draft: R. Wood
Writing – review & editing: R. Wood, M. A. Vogt, I. L. McCoy

aerosol-radiation interactions, that is, changes in clear sky scattering and absorption, and from cloud-mediated effects known as aerosol-cloud interactions (Bellouin et al., 2020). Aerosol-cloud interactions comprise increases in cloud droplet concentration that increase the reflection of sunlight even without cloud macrophysical changes, a phenomenon known as the Twomey effect (Twomey, 1977). In addition, increases in droplet concentration can induce adjustments in cloud condensate (liquid water) and potentially cloud cover (Bellouin et al., 2020; Seinfeld et al., 2016). As aerosol loadings increase, the Twomey effect always produces a negative forcing but cloud adjustments can be positive or negative depending upon the background meteorology and properties of the clouds and boundary layer. Marine low clouds downstream of major industrialized regions have seen declines in cloud droplet concentration (D. T. McCoy et al., 2018) that indicate a reduction in the Twomey effect, and the hemispheric contrast in cloud droplet concentration between the polluted Northern and more pristine Southern Hemispheres has decreased significantly since 2000 (Cao et al., 2023). We are now in an era where the rate of change of aerosol radiative forcing is positive, which ceteris paribus must increase the rate of global warming (Dvorak et al., 2022). Thus, it is important that climate change risk assessments include the impacts of changing atmospheric aerosol and precursor emissions (Persad et al., 2022).

Even with overall emissions fixed, a shift in the emission *location* can change the global aerosol radiative forcing (Persad & Caldeira, 2018), and changes in the efficacy of a given radiative forcing (Hansen et al., 2005) can result in different global mean temperature change per unit of radiative forcing. The Scenario Model Intercomparison Project (ScenarioMIP, O'Neill et al., 2016) within Phase 6 of the Coupled Model Intercomparison Project (CMIP6) provides a suite of plausible future emissions trajectories (shared socioeconomic pathways, SSPs) under different assumptions regarding social and economic development, including climate mitigation efforts. There are very different motivations for air quality cleanup versus climate mitigation efforts, and these are associated with vastly different short term (decadal) costs and benefits to individual nations. Thus, future aerosol changes are not necessarily coupled to future well-mixed greenhouse gas (WMGHG) emissions. The prior two decades are an example of this decoupling: air quality cleanup efforts have proceeded rapidly but mitigation of WMGHG emissions has been extremely limited. This situation may well continue through the next few decades, although this is not at all certain since rapid industrialization of Africa and South America has the potential to stall aerosol emission reductions globally (Feng et al., 2019).

There is a general consensus that the impacts of climate change are likely to become increasingly dire if global warming is allowed to exceed 2C above the preindustrial (IPCC, 2021). In 2020, the global mean temperature of the Earth was close to ∼1.2C above the preindustrial (Morice et al., 2021), and global mean warming rates over the last few decades (NOAA, 2023) have averaged about 0.2 K decade^{-1}. Thus, it is important to quantify the potential impact of different aerosol cleanup policies on the global rate of warming over the coming few decades. Here, we use an 18-member ensemble of ScenarioMIP projections (O'Neill et al., 2016) from CMIP6 models (Eyring et al., 2016) to explore how aerosol cleanup may influence the probability that global warming exceeds 2C by 2050. Section 2 describes the data and methods used. Section 2.2 describes a novel approach that applies the approximate partial radiative perturbation (APRP) method (Taylor et al., 2007) to the multimodel mean output data and partitions future SW radiative changes into temperature-driven and aerosol-driven components, from which we estimate future aerosol radiative forcing and compare it with the published estimates for four shared socioeconomic pathways. Section 3 describes how we use the APRP output to estimate aerosol effective radiative forcing in the SSPs. Section 4 then uses the derived aerosol radiative forcing estimates together with a forcing and response two-level energy balance model (Geoffroy et al., 2013) to explore the impacts of different future aerosol pathways for aerosol cleanup. Section 5 provides an assessment of the implications of the findings and the main conclusions from the study.

2. Materials and Methods

2.1. CMIP6 ScenarioMIP Simulations

Climate model projections from four Tier-1 ScenarioMIP scenarios from CMIP6 are analyzed here. Each scenario has a distinct SSP and level of forcing following the Representative Concentration Pathways (RCPs) used for previous CMIPs (O'Neill et al., 2016; Riahi et al., 2017). The SSPs include differences in societal development related to concerns around climate change. Low numbered SSPs (e.g., SSP1: *Sustainability*, SSP2: *Middle of the Road*) have fewer challenges to climate mitigation while higher SSPs have more (e.g., SSP3: *Regional Rivalry*, SSP5: *Fossil-fueled Development*) (Riahi et al., 2017). Each of the SSPs also includes projections of future

emissions of aerosol and precursor gases. These somewhat parallel the WMGHG changes in that SSPs with aggressive greenhouse gas mitigation tend to have aggressive aerosol reduction. As discussed in the introduction, it is far from clear that there will be such a tight coupling between aerosol and WMGHG mitigation in the coming decades. In this study, we will decouple future changes in aerosol from future changes in WMGHG to allow, for example, an aggressive aerosol cleanup strategy to be applied to less aggressive WMGHG mitigation scenarios (or vice versa).

SSP1-2.6 uses the RCP2.6 pathway, is the most weakly forced scenario considered (experiencing less than 2C warming by 2100 relative to preindustrial in the multi-model mean), and undergoes aggressive aerosol cleanup. SSP2-4.5 undergoes intermediate radiative forcing, is an update to RCP4.5, and has a less rapid reduction in aerosol compared to SSP1-2.6. SSP3-7.0 has a higher radiative forcing (an update to RCP7.0). In particular, it has large land use changes and maintains high emissions of short lived climate forcers (e.g., aerosols) until 2100. Finally, SSP5-8.5 has the strongest overall radiative forcing by 2100 of all the scenarios considered, an update to RCP8.5.

Our analysis focuses on changes between the present day (2015–2025) and the future decades of the 21st century using composites from 18 CMIP6 models (more details in Supporting Information S1). All currently available models with outputs necessary for estimating aerosol contributions to the top of atmosphere (TOA) energy budget are included. We use aerosol optical depth at 550 nm wavelength (*AOD*) as the measure of aerosol loading as it is available for the most models. For reference, global changes in key quantities for the four scenarios by the end of the 21st century are listed in Table S2 of I. L. McCoy et al. (2022).

The trends in *AOD*, which are primarily driven by changes in anthropogenic aerosol emissions (Turnock et al., 2020), differ strongly across the four scenarios (Figure 1a). The trends in the future *AOD* changes in different SSPs are largely independent of global warming trends (Figure 1b) because warming is *primarily* driven by changes in WMGHGs, with a weaker modulation by aerosol. Because CMIP6 models specify aerosol and precursor emissions rather than specifying concentrations, there is considerable spread in aerosol loadings across the models, as indicated by the shaded regions in Figure 1a. Aerosol *trend* differences are most evident over the coming few decades, so we focus primarily on the period 2020–2050, where aerosol cleanup is likely to have the largest impact on warming rates. SSP1-2.6 has the most aggressive reduction in *AOD*, with rapid cleanup occurring prior to 2050, while SSP2-4.5 has a weaker, but steadier decline in *AOD* that extends beyond 2050. SSP3-7.0 essentially has no aerosol mitigation and a very slight upward *AOD* trend over the 21st century. SSP5-8.5 is very similar to SSP2-4.5 prior to 2050 when *AOD* reduction ceases until after 2070. These changes are consistent with projected emissions of aerosol and precursor gases (most importantly SO_2 and VOCs) (Turnock et al., 2020). We can therefore identify three broad *aerosol cleanup pathways*: (a) deep and rapid cleanup (SSP1-2.6); (b) slow and steady cleanup (SSP2-4.5); (c) a slight increase in aerosol (SSP3-7.0).

2.2. Approximate Partial Radiative Perturbation Analysis

Partial radiative perturbation (PRP) analysis (e.g., Colman & McAvaney, 1997) is an offline method to compute feedbacks (e.g., water vapor, lapse rate, cloud, etc.) in response to some forcing from a climate model simulation by examining the TOA radiative changes when the "control" and "perturbed" model fields are interchanged. For PRP, dedicated calls to the model's radiative transfer scheme must be made, and a large volume of model output data is required. A simpler method, that targets contributions to TOA shortwave perturbations, and can be applied to standard (typically monthly mean) model outputs, is known as the approximate PRP (APRP) method first described in Taylor et al. (2007). We use the APRP code provided by Zelinka (2021). The APRP method uses a simplified radiative transfer scheme to apportion changes in TOA SW radiation (ΔSW) to changes in cloudy sky SW (ΔC), non-cloudy sky SW (ΔN), and to changes in surface albedo (ΔS):

$$\Delta SW = \Delta C + \Delta N + \Delta S \tag{1}$$

The APRP method (see also Zelinka et al. (2023) for application) further breaks the cloudy and non-cloudy sky components into respective changes due to scattering and absorption, and, for ΔC, changes in cloud amount (ΔC_{amt}). Surface albedo influences on ΔSW are broken down into changes of surface albedo under cloudy sky (ΔS_{cld}) and non-cloudy sky (ΔS_{clr}) conditions separately:

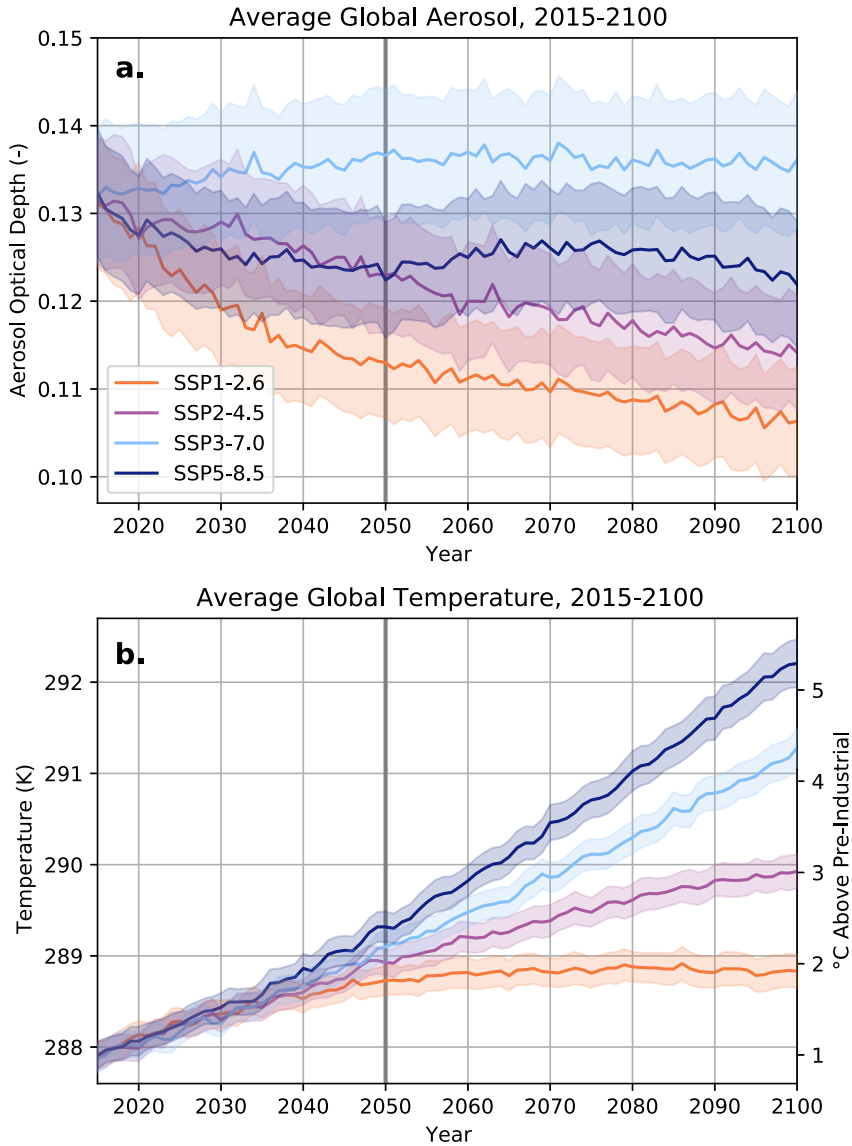

Figure 1. Ensemble annual and global mean (a) aerosol optical depth (*AOD*) and (b) surface air temperature from the CMIP6 models used in this study. For (b), the absolute temperature is indicated on the left axis and the temperature relative to the multimodel mean preindustrial baseline on the right axis.

$$\Delta C = \Delta C_{\text{scat}} + \Delta C_{\text{abs}} + \Delta C_{\text{amt}} \tag{2}$$

$$\Delta N = \Delta N_{\text{scat}} + \Delta N_{\text{abs}} \tag{3}$$

$$\Delta S = \Delta S_{\text{cld}} + \Delta S_{\text{clr}} \tag{4}$$

Figure 2 shows these changes in TOA SW over the 21st century normalized by the global mean surface air temperature changes ΔT over the same period. Importantly, differences in $\Delta SW/\Delta T$ across the four SSPs (solid red bars) are driven primarily by changes in the cloudy sky (ΔC, solid blue bars), with a much smaller influence of variability in the non-cloudy sky and surface albedo. Given that surface air temperature changes over the 21st century vary considerably across the SSPs (Figure 1b; Table S2 in Supporting Information S1), the relative invariance in $\Delta S/\Delta T$ across the SSPs (Figure 2) indicates that surface albedo-driven TOA SW changes are largely a temperature-mediated feedback.

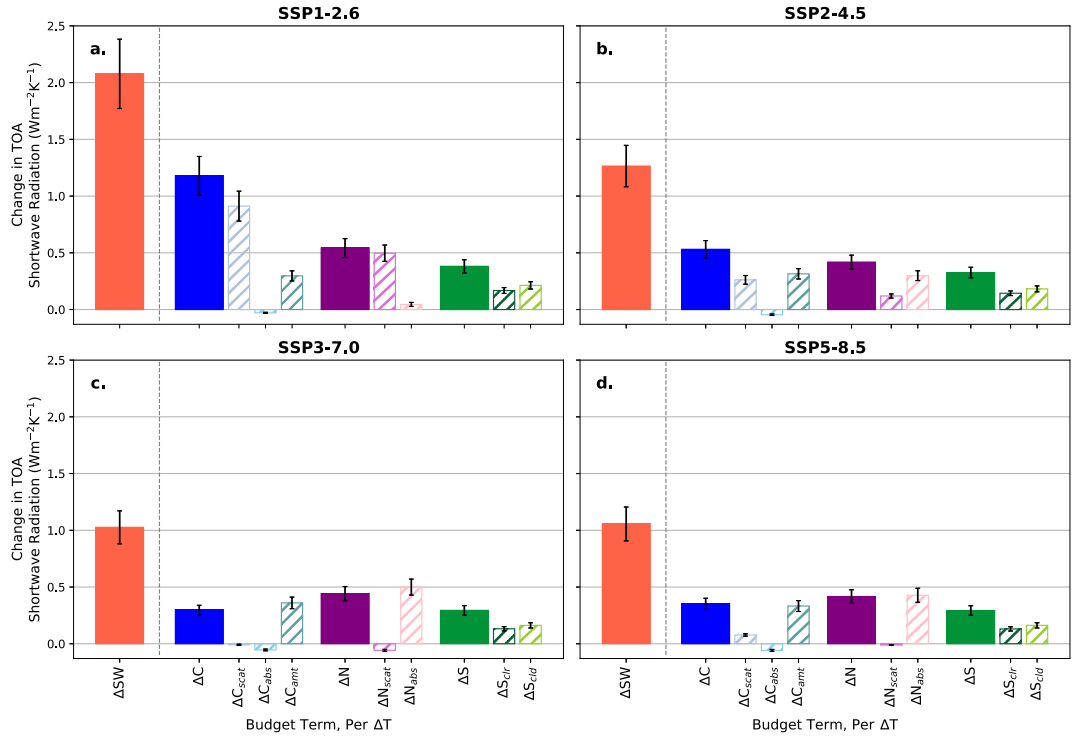

Figure 2. Apportionment of changes in TOA SW radiation (ΔSW, solid red bars) over the 21st century (2090–2100 minus 2015–2025) into changes in cloudy sky (ΔC, solid blue), clear sky (ΔN, solid purple), and changes in surface albedo (ΔS, solid green) deduced from the APRP analysis. Changes are all normalized by the global mean surface air temperature changes over the same period, ΔT. Hatched bars indicate further breakdown of these components (see Equations 2–4). Bars represent multi-model means while error bars show 2 standard errors (~95% confidence) based on the variability in the multi-model mean over the two 10-year periods (2090–2100 and 2015–2025) at the end and the start of the record (Text S1 in Supporting Information S1).

From 2020 to 2100, 99% of the variance in ΔSW across all four SSPs is explained by ΔT and ΔAOD as predictors in a multiple linear regression model (Figure 3). Thus, most of the variance in ΔSW can be explained by a linear sum of a temperature mediated feedback and an aerosol-driven SW response. The predictor variables ΔT and ΔAOD are uncorrelated ($R^2 = 0.01$), so multicollinearity issues (e.g., Qu et al., 2015), where predictor variables are highly correlated, is not a concern here. To further explore the temperature and aerosol-driven SW changes, we also conduct linear regression analysis of the individual component SW changes (ΔC, ΔN, and ΔS) to isolate changes that depend upon ΔAOD from those due to temperature-mediated climate feedbacks (Figure 4). Like that for the overall ΔSW, these individual component regressions (which include all four SSPs) also explain a very high fraction of the variance in the SW APRP components. Each of ΔC, ΔN, and ΔS is regressed against ΔT and ΔAOD. Normalizing by ΔT means that the temperature mediated sensitivities are, by construction, identical across SSPs (Figure 4) because we use all four SSP time series in each regression. Separate regressions for each SSP produce very similar ΔT sensitivities (not shown). Aerosol-mediated changes differ widely across SSPs (Figure 4). The T-mediated components of the SW component changes can be removed to isolate only the AOD-mediated SW changes:

$$\Delta SW_{\mathrm{AOD}} = \Delta SW - \Delta SW_{\mathrm{T}} \tag{5}$$

where here ΔSW can represent either the overall SW change or the individual APRP components.

Aerosol-mediated SW changes differ strongly between SSPs. For example, the AOD-mediated change in cloudy sky TOA SW ($\Delta C_{\mathrm{AOD}}/\Delta T$) is ~0.7 ± 0.1 W m^{-2} K^{-1} in SSP1-2.6, which has deep and rapid aerosol reductions (Figure 4a), but is close to zero for those SSPs with little or no cleanup (SSP3-7.0 and SSP5-8.5). We anticipate that aerosol radiative forcing from aerosol-radiation interactions is likely to partly scale with overall aerosol loading, yet the AOD dependence of the non-cloudy sky APRP component ($\Delta N_{\mathrm{AOD}}/\Delta T$) is close to zero *for all*

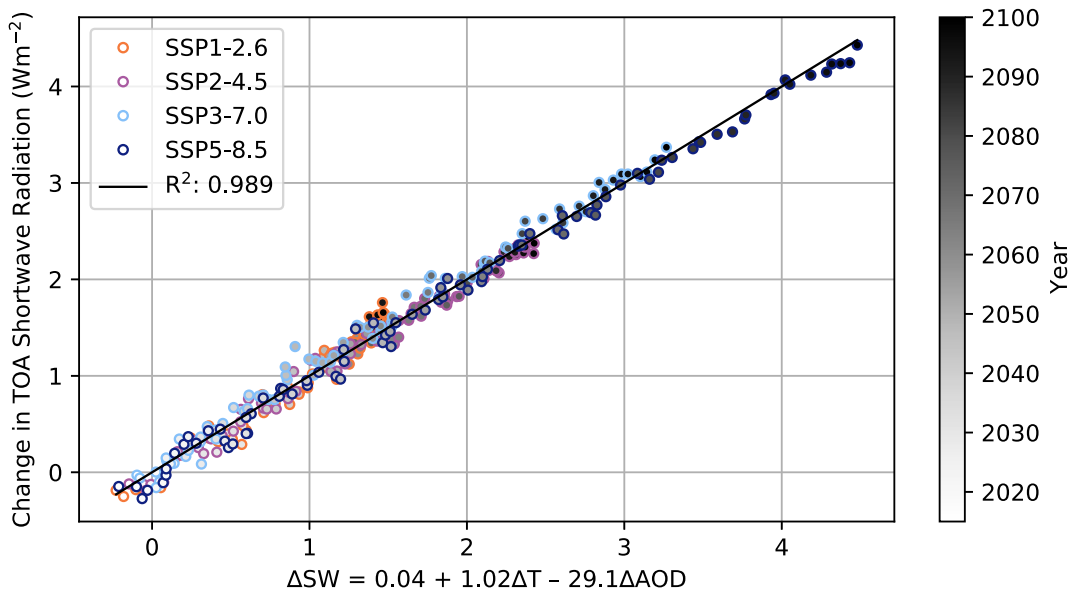

Figure 3. Annual mean TOA SW differences from the average of those in 2015–2025 (ΔSW) plotted as a function of annual mean ΔAOD and ΔT. A single regression line is fitted, explaining 99% of the variance using ΔT and ΔAOD as predictors.

SSPs (rightmost purple hatched bars in Figure 4). Below, we demonstrate that near-complete cancellation between changes in scattering and absorbing aerosol are responsible for $\Delta N_{\mathrm{AOD}} \sim 0$.

To gain further insights into processes controlling ΔSW, we present the regressions of the cloudy and clear APRP components (ΔC and ΔN) in Figures 5 and 6 respectively. The equivalent figure for surface albedo changes is

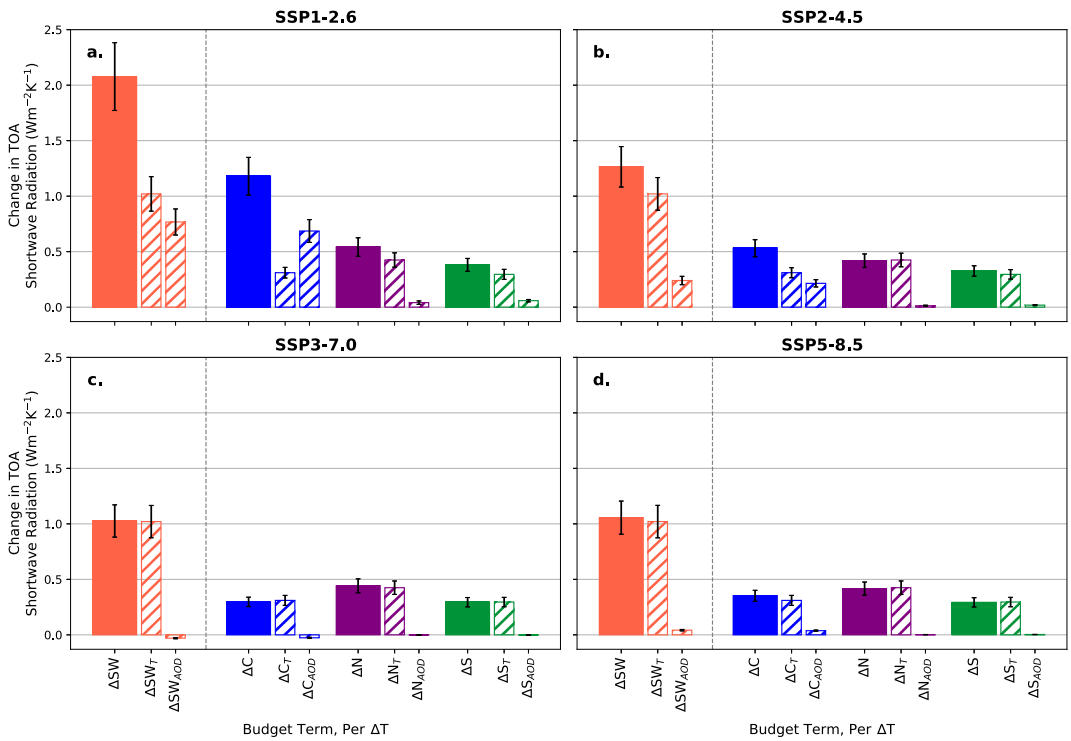

Figure 4. As in Figure 2 but showing APRP component contributions to TOA SW changes over the 21st century that are associated with changes in ΔAOD and ΔT. Note that the TOA SW changes are normalized by ΔT here, so that T-mediated sensitivities are identical across all SSPs.

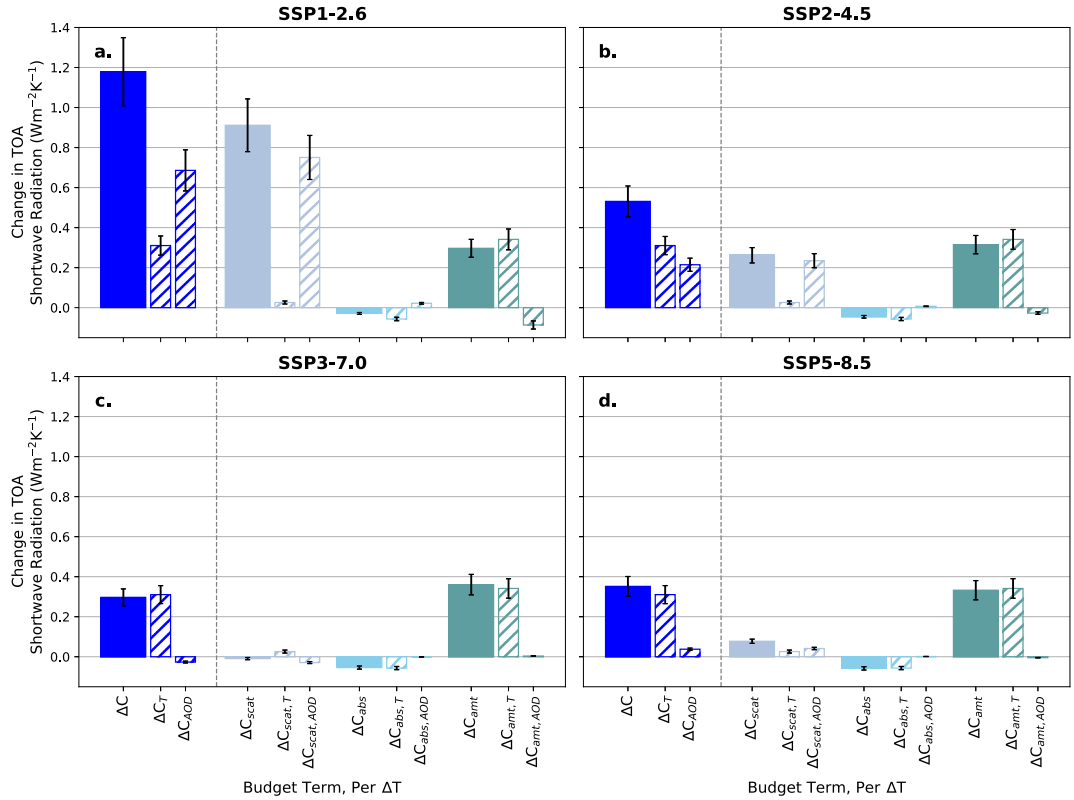

Figure 5. As in Figure 2, but for the breakdown of cloudy sky SW changes ΔC (solid blue bar at left) into scattering (solid gray), absorption (solid sky blue), and cloud amount (solid teal) components. Each component is regressed against ΔT and ΔAOD and those dependencies are provided, respectively, in the hatched bars to the right of the solid bars.

provided in Figure S1 of the Supporting Information S1 but is not discussed further as ΔS sensitivity to aerosol is negligible. It is striking that almost all of the cloudy sky scattering (ΔC_{scat}, gray bars) variability across SSPs can be explained by ΔAOD, whereas cloud amount changes (ΔC_{amt}, teal bars) are almost all explained by ΔT (Figure 5). Changes in cloudy sky absorption (ΔC_{abs}, sky blue bars) are much smaller than those in either scattering or cloud amount and are more associated with ΔT than ΔAOD. We interpret the T-driven cloud amount decreases ($\Delta C_{\text{amt,T}}$) as the expected positive cloud feedback to warming temperatures, and the AOD-driven decreases in cloudy sky scattering ($\Delta C_{\text{scat,AOD}}$) as radiative forcing from a combination of the Twomey effect and adjustments in liquid water. The positive SW cloud amount feedback of $\sim 0.35 \pm 0.05$ W m^{-2} K^{-1} over this period ($\Delta C_{\text{amt,T}}$, first hatched teal bar in all Figure 5 panels) is consistent with cloud feedback estimates determined from observations (Sherwood et al., 2020) and from CMIP6 models (Zelinka et al., 2020). Given that we are using a very different approach for determining model cloud feedbacks from those typically used (i.e., abrupt 4 × CO_2 simulations), this excellent agreement provides confidence in our APRP methodology for isolating cloud changes due to aerosol from those due to warming.

The lack of an aerosol signature in the non-cloudy sky SW changes (i.e., $\Delta N_{\text{AOD}} \sim 0$ in Figure 4) occurs despite significant changes in aerosol in the different SSPs. We further separate ΔN into scattering and absorbing components in Figure 6 to understand this behavior. Both ΔN_{scat} and ΔN_{abs} are strongly associated with ΔAOD (pink and peach hatched bars in Figure 4) but the two effects almost exactly cancel each other. Because scattering components (primarily sulfate and organic carbon) and absorbing components (primarily black carbon) are often co-emitted, aerosol cleanup policies typically result in reductions in both scattering and absorbing components. A high degree of cancellation was also noted in Bond et al. (2013). Finally, we note that $\Delta N_{\text{abs,T}} \sim 0.5$ W m^{-2} K^{-1}. This can be attributed to increasing SW absorption by water vapor in a warmed climate (e.g., I. L. McCoy et al., 2022; Pendergrass & Hartmann, 2013).

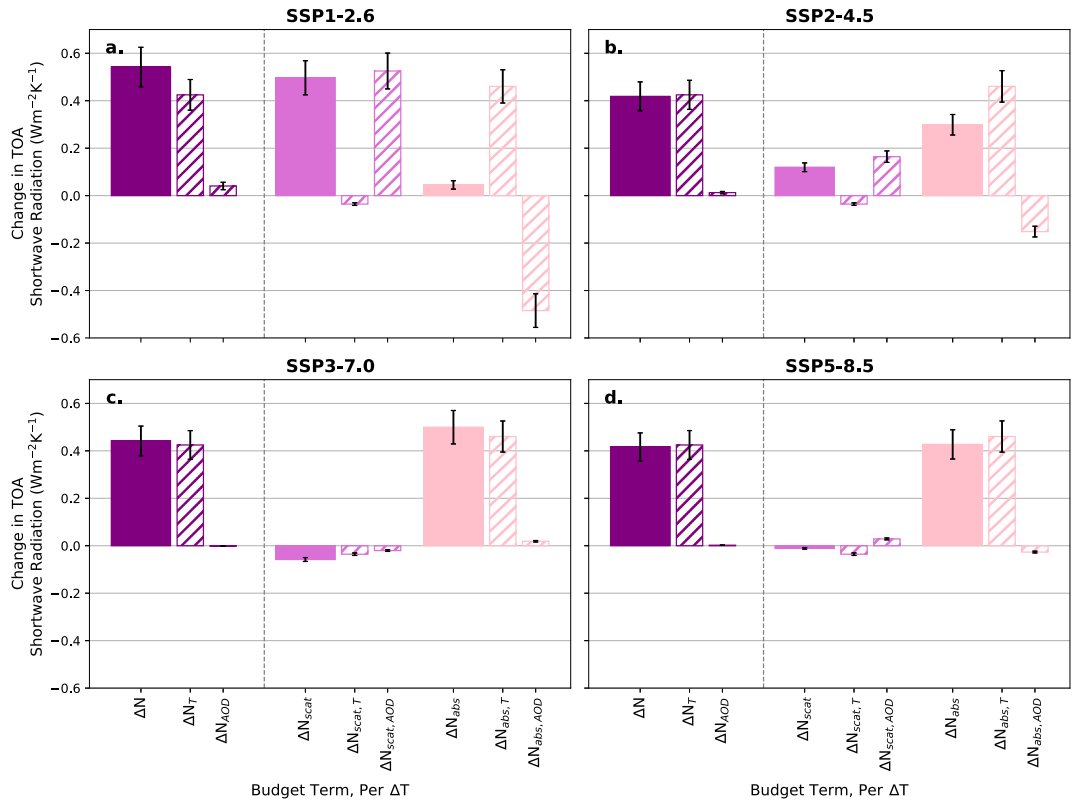

Figure 6. As in Figure 2, but for the breakdown of non-cloudy sky SW changes ΔN (solid purple bar at left) into scattering (solid pink) and absorption (solid peach) components. Each component is regressed against ΔT and ΔAOD and those dependencies are provided, respectively, in the hatched bars to the right of the solid bars.

The small ΔN_{AOD} indicates negligible net SW radiative forcing from aerosol-radiation interactions. This means the vast majority of aerosol SW radiative forcing in the CMIP6 models is cloud-mediated, driven by changes in cloud scattering rather than changes in cloud amount. The overall SW aerosol effective radiative forcing (ERF) is the sum of ERF for aerosol-cloud interactions plus aerosol-radiation interactions, that is, $ERF_{\mathrm{aer}} = ERF_{\mathrm{aci}} + ERF_{\mathrm{ari}}$, and is determined as the sum of the AOD dependencies of the individual APRP components:

$$ERF_{\mathrm{aer}} = ERF_{\mathrm{aci}} + ERF_{\mathrm{ari}} = \Delta SW_{\mathrm{AOD}} \approx \Delta C_{\mathrm{AOD}} + \Delta N_{\mathrm{AOD}} + \Delta S_{\mathrm{AOD}} \quad (6)$$

We use the sum of the three AOD regressions of the separate contributing terms (i.e., ΔC_{AOD}, ΔN_{AOD}, and ΔS_{AOD}) as our estimate of SW ERF_{aer}. A multiple regression of the sum of the terms, that is, ΔSW, against T and AOD, leads to an estimate of SW ERF_{aer} that is only 2% different. Based on our findings that ΔN_{AOD} and ΔS_{AOD} are both close to zero, $ERF_{\mathrm{aci}} + ERF_{\mathrm{ari}} \approx ERF_{\mathrm{aci}} \approx \Delta C_{\mathrm{AOD}} \approx \Delta C_{\mathrm{scat,AOD}}$. Thus, practically all of the SW ERF_{aer} over the 21st century can be attributed to cloud scattering changes (i.e., the Twomey effect and liquid water path adjustments). The dominant contribution of ERF_{aci} to ERF_{aer} is consistent with behavior for the 20th century (Zelinka et al., 2023).

3. Aerosol Effective Radiative Forcing in the SSPs

The SW ERF_{aer} determined using the APRP-regression approach described in Section 2.2 is shown as a time series in Figure 7 in preparation for comparing to ERF_{aer} estimates from the literature. As part of the ScenarioMIP project, multi-model mean time series of net (SW + LW) ERF_{aci} and ERF_{ari} are generated using an emulation-based calibration technique (Lund et al., 2019; Meinshausen et al., 2011) applied to 17 CMIP6 models (Leach et al., 2021). These annual mean effective radiative forcing time series from the SSPs are taken from tables provided in Smith et al. (2021), henceforth S21. We subtract the 2015–2025 mean so that the ERF_{aer} is relative to the 2020 baseline rather than to the preindustrial. Note that Zelinka et al. (2023) found significant biases in the

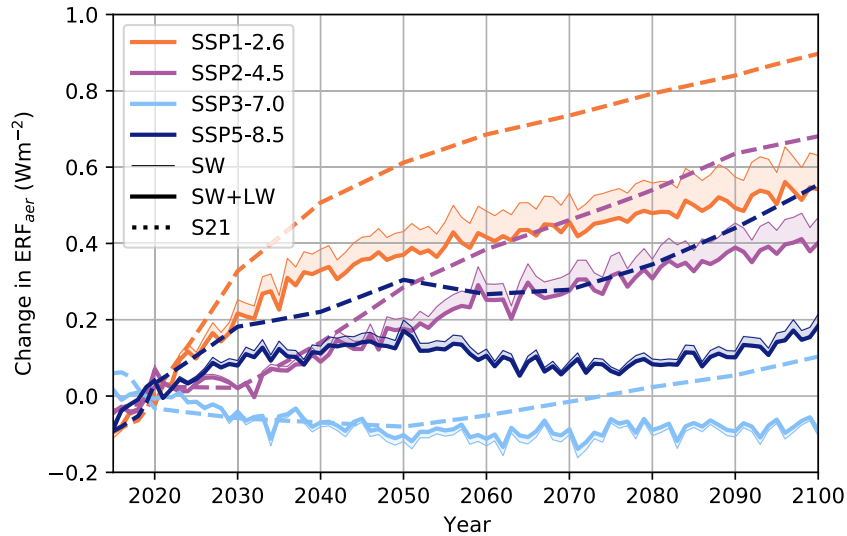

Figure 7. Time series of aerosol effective radiative forcing(ERF_{aer}) from the APRP method described in this work (thick solid lines show SW + LW, thin solid lines are SW only, and the shading marks the LW contribution) and from the CMIP6 multi-model ensemble emulation method of Smith et al. (2021) (thick dashed lines show SW + LW). All forcings are shown relative to a 2020 (2015–2025) baseline.

separate ARI and ACI APRP components, but that the total (ARI + ACI) radiative forcing is only minimally biased. In this paper, we only use the total aerosol radiative forcing from S21.

It is important to note that our APRP-regression approach does not provide an estimate of LW ERF_{aer}, which is necessary for comparing to the S21 net ERF_{aer}. To make an assessment of the LW aerosol radiative forcing over the 21st century, we adopt an alternative regression technique. The multimodel ensemble change in TOA net LW radiation (ΔLW) is the sum of changes due to WMGHG radiative forcing agents active in the LW ($\Delta F_{\mathrm{WMGHG}}$), a temperature-dependent response (ΔLW_{T}) due to warming temperatures and changing water vapor, and a component ΔLW_{AOD} representing aerosol-induced TOA LW changes:

$$\Delta LW = \Delta F_{\mathrm{WMGHG}} + \Delta LW_{\mathrm{AOD}} + \Delta LW_{\mathrm{T}} \tag{7}$$

The radiative forcing time series $\Delta F_{\mathrm{WMGHG}}$ is taken from S21 and includes CO_2, CH_4, N_2O, and other well-mixed greenhouse gases. These are removed from ΔLW, after which the AOD and T dependent components (ΔLW_{AOD} and ΔLW_{T} respectively) are determined using multiple linear regression against ΔAOD and ΔT.

Figure 7 shows that accounting for the net (SW + LW) estimated aerosol radiative forcing from this study instead of only the SW ERF_{aer} *increases* the aerosol forcing discrepancy between S21 and our estimation by approximately 25%. This is consistent with expectations that LW ERF_{aer} will be the opposite sign to the SW ERF_{aer}. Consider the radiative forcing from a negative cloud liquid water path (LWP) adjustment, which is a typical GCM response to decreasing aerosol (Bellouin et al., 2020). In the SW, this decreases sunlight reflection (positive forcing), but will increase the overall LW emission because the underlying surface is warmer than the clouds above (negative forcing). Zelinka et al. (2023) assesses a LW ERF of 0.16 W m^{-2} (±0.34 W m^{-2}) for the present day (2014) minus the preindustrial in CMIP6 models. In that study the multimodel SW ERF_{aer} is −1.25 W m^{-2}. If the 21st century LW ERF_{aer} scales similarly with the SW ERF_{aer}, then for a SW ERF_{aer} of 0.6 W m^{-2} (the approximate SW forcing from 2020 to 2100 in SSP1-2.6, Figure 7) the LW forcing would be approximately −0.08 W m^{-2}. This is very close to the −0.06 W m^{-2} we deduce from the regression analysis described above. We note that these LW ERF_{aer} estimates have large relative uncertainty (>100%) but have small absolute magnitude.

The APRP-derived and S21 ERF_{aer} series for each SSP exhibit similar curves but with an offset between their values that increases approximately linearly with time (Figure 7). We find that the S21 forcing increases over the 21st century are approximately 0.20–0.35 W m^{-2} larger than those from the APRP approach. By 2090–2100, SSP1-2.6 ERF_{aer} values are 0.87 W m^{-2} (S21) and 0.61 W m^{-2} (APRP) which is equivalent to a ∼40% difference in relative terms.

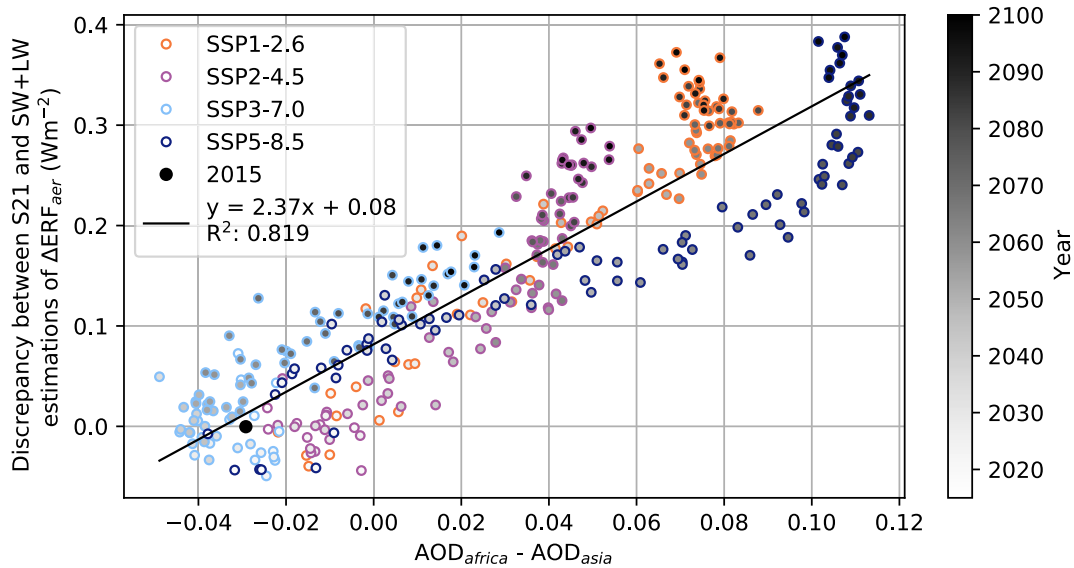

Figure 8. Difference between the S21 and APRP-derived ERF_{aer} regressed against the difference in *AOD* between a region in Equatorial Africa and East Asia (see text). The symbol shading indicates the year (see bar at right), with the initial value (2015) shown with the solid circle.

There are two possible reasons that may help to explain why ERF_{aer} from S21 increases more rapidly than from the APRP approach used in this study. Both relate to the model calibration for S21. First, it is important to note that the suite of models used here and in S21 is not identical. Although many of the CMIP6 models used in the APRP analysis are the same models as used in S21, and others are close variants of those used in S21, there are a few models in each suite that are not present in the other. Our approach does not enable a harmonization of the models used. A second source of possible discrepancy is that the S21 ERF_{aer} is derived from model simulations covering the historical record, and specifically comparing the year 2014 with a preindustrial (PI) control (Smith et al., 2021). The model calibration parameters are then applied to model output data over the 21st century. However, as noted in the introduction, model experimentation has demonstrated that changing the geographic distribution of aerosol-impacting emissions can result in a different radiative forcing for the same total magnitude of emissions (Persad & Caldeira, 2018).

To investigate these potential reasons in more detail, we first note that the S21 multi-model mean ERF_{aer} (LW + SW) for 2014 minus the PI is -1.01 W m^{-2} with a standard deviation across the models of 0.23 W m^{-2}. Zelinka et al. (2023) applied the APRP method to historical simulations (2014 minus PI) with a similar model suite as we use for the 21st century and obtained an estimate of ERF_{aer} for the same period as S21 (2014 minus the PI) of -1.09 W m^{-2} with a standard deviation of 0.24 W m^{-2}. The similarity in the multimodel forcing mean and spread between these two studies provides some confidence that different model selection between the approaches in S21 and our study is probably *not* responsible for the forcing differences in Figure 7 as they are examined relative to their respective baselines.

To investigate the possibility that changes in the *location* of the key emission regions may be responsible for some of the ERF_{aer} discrepancy between the S21 and our APRP estimates (Figure 7), we introduce a metric that is sensitive to a geographic shift of major emission regions in the present day (2015–2025) and the later part of the 21st century. One can argue that the rise of emissions in SE Asia occurred prior to 2014 and so these emissions are well-reflected in the model calibration used in S21. On the other hand, the 21st century is likely to see a shift in the main anthropogenic emission regions as cleanup policies start to take effect in East Asia while the emissions in rapidly industrializing Africa may remain relatively flat (Turnock et al., 2020). We find that the difference in *AOD* between a large region of East Asia (0–45°N, 60–130°E) and Equatorial Africa (15°S–15°N, 30°W–30°E), that is, AOD_{Africa}-AOD_{Asia}, explains just over 80% of the variance in the S21-APRP discrepancy in ERF_{aer} (Figure 8). It seems reasonable to postulate that much of the discrepancy between the APRP and S21 estimates of ERF_{aer} over the 21st century can likely be attributed to shifting emission locations. Thus, it is important that future work explores how different emission locations may impact not only regional temperature responses but also the global

mean response. For the 21st century temperature responses (Section 4), we will use both forcing estimates in our calculations, with differences between the two providing a measure of the impact of aerosol forcing uncertainty on future warming.

4. Temperature Responses

For each of the four SSPs, the ERF_{aer} time series using the APRP method (Figure 7) are used together with all other anthropogenic radiative forcings (taken from Smith et al. (2021)) to estimate a future global mean surface air temperature time series projection. As motivated in the introduction, we decouple future changes in aerosol from future changes in all other anthropogenic forcings (predominantly WMGHGs). This is achieved by considering the 16 potential combinations of aerosol forcing (ERF_{aer}) from one of the four SSPs with all other anthropogenic forcings (ERF_{other}) taken from another SSP. In this way, we can consider the effect of different aerosol cleanup strategies on scenarios that involve different levels of decarbonization. For example, we can examine the effects of rapid aerosol cleanup on a future with very limited decarbonization by pairing the future aerosol forcing from SSP1-2.6 with other anthropogenic aerosol forcings taken from SSP5-8.5.

Global annual mean temperature time series from 1750 to 2100 are calculated using the simple two-layer climate model used in Dvorak et al. (2022) and a very similar approach to Geoffroy et al. (2013). For each of 100,000 ensemble members, model parameters are drawn randomly from normal distributions as specified in Dvorak et al. (2022), with the same truncation of the deep ocean heat capacity to avoid very small values. Instead of using a uniform distribution of equilibrium climate sensitivity (ECS) as in Dvorak et al. (2022), we draw from a normal distribution for the climate feedback parameter with mean and standard deviation of 1.20 W m^{-2} K^{-1} and 0.26 W m^{-2} K^{-1}, respectively. This gives a 50th percentile ECS value of 3.1 K, with 5th and 95th percentiles of 2.3 and 4.8, respectively, which are very close to those assessed in Sherwood et al. (2020). Radiative forcings and resulting temperatures are all taken relative to 2020 values.

An example showing input radiative forcings and output decadal mean temperature responses is shown in Figure 9. In this case, ERF_{aer} is taken from SSP1-2.6 which experiences a deep and rapid decrease in aerosol forcing magnitude from the present day out to ~2040 (also see Figure 7). The other, non-aerosol radiative forcings for this example are taken from SSP2-4.5. The ramp-up in aerosol forcing magnitude over the second half of the 20th century is followed by cleanup over the early 21st century, leading to a 50-year delay in global warming (Figure 9b). Warming rates over the period 2020–2050 are 20%–40% greater with aerosol cleanup than without. This highlights the critically important contribution of aerosol cleanup to near-term warming rates.

Figure S2 in Supporting Information S1 compares global mean temperature time series taken from the 18 member ScenarioMIP CMIP6 global model ensemble with those from the simple climate model. For each of the four SSPs, the simple climate model projected median temperature increase agrees very well with the CMIP6 multimodel mean, providing confidence in the simple climate model projections.

Cumulative probability distributions of projected global mean surface air temperature warming rates over the three decade period 2020–2050 are shown in Figure 10 for different combinations of ERF_{aer} and ERF_{other} taken from the SSPs. The cdf spread expresses the overall uncertainty in the simple climate model calibration (ocean heat uptake, climate feedback, Geoffroy et al. (2013)) plus a statistical sampling uncertainty. Intermodel uncertainty in aerosol forcing, which we estimate by assuming its relative uncertainty is equal to the intermodel spread in AOD change, adds additional error but does not change the results considerably. The global mean temperature in 2020 is approximately +1.2C above the preindustrial (Morice et al., 2021). Given this, additional warming of 0.8C over the period 2020–2050 (a mean warming rate of 0.27 C $decade^{-1}$) would lead to a global mean surface air temperature that reaches 2C above the preindustrial, a threshold that nations have pledged not to exceed as part of the 2015 Paris Climate Agreement. Climate change risks increase dramatically if the 2C threshold is surpassed (IPCC, 2022).

Possible aerosol cleanup pathways over 2020–2050 have significant impacts on warming rates over that period (Figure 10). For example, with strong mitigation of carbon emissions (ERF_{other} from SSP1-2.6), slow (purple) or no (blue) aerosol cleanup likely leads to temperatures that remain below 2C by 2050 (Figure 10a). However, even with strong decarbonization commitments, deep and rapid aerosol cleanup results in a 5% chance (APRP) to a 12% chance (S21) of reaching 2C by 2050 (orange curves).

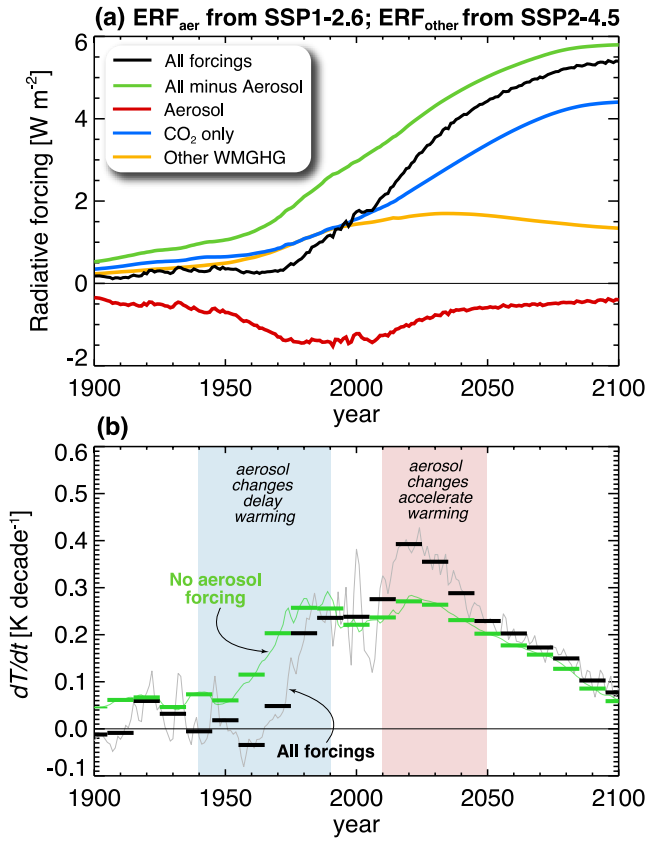

Figure 9. Example of (a) radiative forcings, and (b) predicted decadal temperature trends from the simple two-layer climate model. The model is run with all forcings (black) and with all forcings except the aerosol radiative forcing (green). In this case, the aerosol forcing series is taken from our APRP method applied to SSP1-2.6 (see Figure 7). The non-aerosol (other) forcings are taken from SSP2-4.5. In (a), the greenhouse forcing is broken down into that from CO_2 (blue) and from other WMGHGs (orange), which together account for almost all of the non-aerosol radiative forcing (green). Panel (b) shows the annual warming rate (thin lines) and the decadal mean warming rates (horizontal bars). Aerosol increases during the period from ~1940 to ~1990 dramatically reduced the warming over that period, whereas from 2010 to 2050 the deep and rapid cleanup associated with the SSP1-2.6 future aerosol trend leads to a considerable acceleration of the warming.

Given current, nationally determined contributions to decarbonization, it is unlikely that greenhouse gas radiative forcing will follow the specifications of SSP1-2.6 and will more likely track those in SSP2-4.5 (Liu & Raftery, 2021). In this case, aerosol cleanup choices profoundly impact the probability of remaining below 2C by 2050 (Figure 10b). With ERF_{other} from SSP2-4.5, aggressive aerosol cleanup (orange curves, i.e., ERF_{aer} from SSP1-2.6) more than doubles the probability of reaching 2C by 2050 from 20% to 30% (blue curves, i.e., ERF_{aer} from SSP3-7.0) to over 75% (Figure 10b). This range indicates that aerosol cleanup choices over the next few decades can make the difference between achieving a 2C target and missing it. It is likely that both of the unmitigated carbon emission scenarios SSP3-7.0 and SSP5-8.5 will exceed 2C by 2050, although aggressive aerosol mitigation makes this outcome almost a certainty.

As explored in Section 3, the APRP method produces a weaker increase in ERF_{aer} than for S21, which likely stems from the shifting geographic location of the aerosol emissions. Thus, regional shifts in aerosol emission locations over the 21st century may be somewhat buffering the overall effects of aerosol cleanup. These regional shifts appear to have a significant impact on global warming rates in addition to any local effects that are induced. This result is consistent with Persad and Caldeira (2018) and strongly warrants a concerted effort to better constrain future aerosol forcing changes (Persad et al., 2022). In addition to shifts in emission locations potentially adding uncertainty to the likelihood of exceeding 2C by 2050, one can also use Figure 10 to estimate the warming rates if aerosol forcing is significantly weaker than the estimates in Figure 7. This might occur should the peak magnitude of the aerosol forcing be less than that estimated here (and in CMIP6 in general). The thin dotted lines in Figure 10 show lower exceedance probabilities for 2C by 2050 assuming zero aerosol forcing, which can be interpreted as the outcome of cleanup attempts should aerosols be found not to provide strong climate cooling.

5. Discussion and Conclusions

The results presented here demonstrate that global warming rates over the next few decades (2020–2050) will be altered significantly by air quality policies designed to reduce the negative health consequences of particulate matter. Note that the analysis in this study does not address the magnitude of health-related benefits that society would also experience under aerosol and precursor reduction polices (Murray et al., 2020).

One of the shortcomings of analyses with simple climate models, such as the one used to estimate temperature responses here, is that natural internal variability in the climate system is not taken into account. Each of the CMIP6 models includes (random) internal variability which is lost when taking the multimodel mean. In future studies, a large ensemble of simulations for one model could be used to carry out the assessment of how much internal variability might affect the results. One could potentially use the CESM Large Ensemble Project Phase 2 (LENS2), but the warming rates for the ensemble are only available for the SSP3-7.0 scenario which has very small aerosol changes over the 21st century. Thus, with this ensemble we would not be able to determine the spread in warming rates across an ensemble that experiences significant future aerosol changes. This is therefore left for future analysis.

There are major uncertainties in aerosol radiative forcing, so the consequences of aerosol cleanup policies on climate could potentially be relatively small. On the other hand, the rapid cleanup of particulate-forming emissions that began in the early 2000s may control the success or failure of the 2015 Paris Climate Agreement to restrict global mean surface air temperatures to no more than 2C above the preindustrial. Thus, it is imperative that aerosols be included in climate risk assessments.

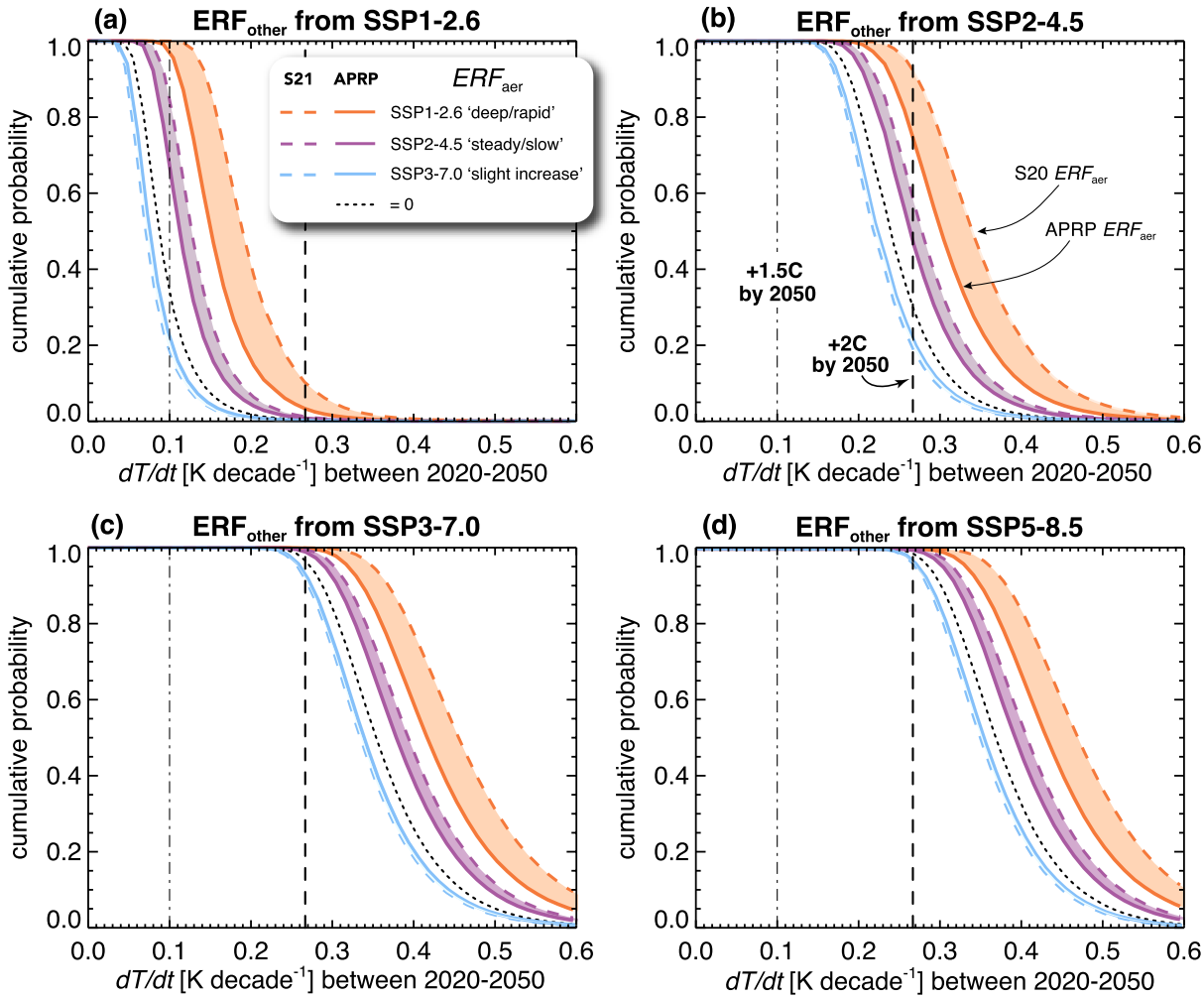

Figure 10. Probability that the global mean surface decadal warming rate over the period 2020–2050 will exceed the value on the abscissa. Temperature is calculated from the ensemble of simple climate models described in Section 4. Different line colors within each panel represent different aerosol pathways: deep and rapid cleanup (orange, SSP1-2.6), steady and slow cleanup (purple, SSP2-4.5), slight increase (light blue, SSP3-7.0), and a case with exactly zero aerosol forcing (black dotted line, $ERF_{aer} = 0$). Each panel presents a different pathway for the other anthropogenic forcings: (a) SSP1-2.6, (b) SSP2-4.5, (c) SSP3-7.0, and (d) SSP5-8.5. The solid and dashed lines for each aerosol pathway represent the ERF_{aer} taken from the APRP method and from S21 respectively, and so the shaded regions represent uncertainty in the aerosol forcing estimate used. Results with aerosol from the SSP5-8.5 scenario are almost identical to those from the SSP2-4.5 scenario, so are omitted. Vertical lines indicate the warming rates required to reach 2C (dashed) and 1.5 C (dash-dot) above preindustrial levels by 2050.

Our findings are broadly consistent with the analysis of Watson-Parris and Smith (2022), wherein the effects of different assumptions about how uncertainty in how effective aerosol radiative forcing will change over the coming decades were found to influence whether climate warming targets may be met. A novel aspect of our study is that we show that shifts in the location of aerosol emissions over the coming decades may also have an important influence on the magnitude of global warming due to aerosol cleanup policies. Shifting emission locations in the coming decades likely renders the relationship between global emissions and ERF_{aer} somewhat nonlinear, motivating further studies on the connection between emission locations and the susceptibility of downwind cloud fields in order to better project how future, changing aerosol and precursor emissions project onto global warming (Persad & Caldeira, 2018; Wilcox et al., 2023). Our results suggest that 21st century changes in emission locations may somewhat reduce the probability of exceeding the 2C target compared to a world where emission locations do not change relative to 2014 emissions patterns. However, there are still significant questions about which countries will adopt stringent cleanup policies and which may not, so that future aerosol emission strengths and locations may be different from those represented in the CMIP6 ScenarioMIP SSPs.

Although a significant additional source of uncertainty in future aerosol forcing appears to be the emission pattern rearrangements, other sources of uncertainty include how cloud macrophysical responses (adjustments) to aerosol are handled in models, which involves understanding how light rain responds to aerosol, how cloud top mixing responds, and how clouds organize their spatial structure. These are varied in terms of how they are (or are not) represented in low dimensional climate models. Cloud locking experiments, in which aerosol source locations are rearranged but where the types of cloud responses allowed are restricted, could be very helpful for understanding how the aerosol direct effect may also be playing an important role in determining the sensitivity of forcing to geographically shifting emissions. These additional studies could be conducted with a single climate model or with multiple models, which is the goal of the Regional Aerosol Model Intercomparison Project (RAMIP, Wilcox et al. (2023)).

In the CMIP6 models, we find that most of the aerosol radiative forcing change in coming decades is driven by radiative forcing from aerosol-cloud interactions. There is increasing focus in recent years on the idea of deliberately introducing aerosol particles into marine clouds with the view of increasing their reflection of sunlight to cool the Earth. This possible climate intervention strategy, known as *marine cloud brightening* (Latham et al., 2012; Wood, 2021), aims to produce a negative ERF_{aer} from aerosol-cloud interactions in marine low clouds. The climate efficacy of marine cloud brightening is currently not well understood (e.g., Stjern et al., 2018) and there are no existing protocols for incorporating marine cloud brightening into the SSP approach. In Figure S4 of the Supporting Information S1 we show a version of Figure 10 that includes how warming probabilities change if solar radiation modification is applied with a constant radiative forcing of -2 W m^{-2} from the year 2030 until 2050 after initially following a deep and rapid aerosol cleanup scenario (SSP1-2.6). With such aerosol forcing, it may be possible to stave off reaching the 2C threshold by 2050 even for those scenarios with greater GHG increases (SSP3-7.0 and SSP5-8.5). Given the importance of emission location shown in this study, efforts to develop realistic climate intervention scenarios are important, in particular for marine cloud brightening whose emission geography would be very different from that due to changing anthropogenic activities.

Data Availability Statement

All CMIP6 ScenarioMIP simulations used in this study are available from the Earth System Grid Federation at https://esgf-node.llnl.gov/search/cmip6/. For the APRP analysis, we use the software from Zelinka (2021).

Acknowledgments
The authors thank Dargan Frierson for helping to identify and download CMIP6 data used in this study, and for providing useful guidance on the use of the simple climate model. We also thank Geeta Persad for insightful discussions and acknowledge the World Climate Research Programme and its Working Group on Coupled Modeling for coordinating CMIP6; the climate modeling groups involved for their simulations; the Earth System Grid Federation (ESGF) for archiving and facilitating data usage; and the multiple funding agencies who support CMIP and ESGF efforts. Research by ILM was supported by the NOAA Climate and Global Change Postdoctoral Fellowship Program, administered by UCAR's Cooperative Programs for the Advancement of Earth System Science (CPAESS) under award NA18NWS4620043B and the NOAA cooperative agreements NA17OAR4320101 and NA22OAR4320151. MAV and RW were funded on indirect cost recovery support from grants to UW. We thank our editor, Jesse Kroll, and three anonymous reviewers for their insights and suggestions for improving our manuscript.

References

Bellouin, N., Quaas, J., Gryspeerdt, E., Kinne, S., Stier, P., Watson-Parris, D., et al. (2020). Bounding global aerosol radiative forcing of climate change. *Reviews of Geophysics*, *58*(1), e2019RG000660. https://doi.org/10.1029/2019RG000660

Bond, T. C., Doherty, S. J., Fahey, D. W., Forster, P. M., Berntsen, T., DeAngelo, B. J., et al. (2013). Bounding the role of black carbon in the climate system: A scientific assessment: Black carbon in the climate system. *Journal of Geophysical Research: Atmospheres*, *118*(11), 5380–5552. https://doi.org/10.1002/jgrd.50171

Cao, Y., Zhu, Y., Wang, M., Rosenfeld, D., Liang, Y., Liu, J., et al. (2023). Emission reductions significantly reduce the hemispheric contrast in cloud droplet number concentration in recent two decades. *Journal of Geophysical Research: Atmospheres*, *128*(2), e2022JD037417. https://doi.org/10.1029/2022JD037417

Colman, R. A., & McAvaney, B. J. (1997). A study of general circulation model climate feedbacks determined from perturbed sea surface temperature experiments. *Journal of Geophysical Research*, *102*(D16), 19383–19402. https://doi.org/10.1029/97JD00206

Dvorak, M. T., Armour, K. C., Frierson, D. M. W., Proistosescu, C., Baker, M. B., & Smith, C. J. (2022). Estimating the timing of geophysical commitment to 1.5 and 2.0°C of global warming. *Nature Climate Change*, *12*(6), 547–552. https://doi.org/10.1038/s41558-022-01372-y

Eyring, V., Bony, S., Meehl, G. A., Senior, C. A., Stevens, B., Stouffer, R. J., & Taylor, K. E. (2016). Overview of the coupled model intercomparison project phase 6 (CMIP6) experimental design and organization. *Geoscientific Model Development*, *9*(5), 1937–1958. https://doi.org/10.5194/gmd-9-1937-2016

Feng, L., Smith, S. J., Braun, C., Crippa, M., Gidden, M. J., Hoesly, R., et al. (2019). Gridded emissions for CMIP6. *Geoscientific Model Development Discussions*, 1–25. https://doi.org/10.5194/gmd-2019-195

Geoffroy, O., Saint-Martin, D., Olivié, D. J. L., Voldoire, A., Bellon, G., & Tytéca, S. (2013). Transient climate response in a two-layer energy-balance model. Part I: Analytical solution and parameter calibration using CMIP5 AOGCM experiments. *Journal of Climate*, *26*(6), 1841–1857. https://doi.org/10.1175/JCLI-D-12-00195.1

Hansen, J., Sato, M., Ruedy, R., Nazarenko, L., Lacis, A., Schmidt, G. A., et al. (2005). Efficacy of climate forcings. *Journal of Geophysical Research*, *110*(D18), D18104. https://doi.org/10.1029/2005JD005776

IPCC. (2021). In V. Masson-Delmotte, P. Zhai, A. Pirani, S. L. Connors, C. Péan, S. Berger, et al. (Eds.), *Climate change 2021: The physical science basis. Contribution of working group I to the sixth assessment report of the Intergovernmental Panel on Climate Change*. Cambridge University Press. https://doi.org/10.1017/9781009157896

IPCC. (2022). In H.-O. Pörtner, D. C. Roberts, M. Tignor, E. S. Poloczanska, K. Mintenbeck, A. Alegría, et al. (Eds.), *Climate change 2022: Impacts, adaptation and vulnerability. Contribution of working group II to the sixth assessment report of the Intergovernmental Panel on Climate Change* (3056 pp.). Cambridge University Press. https://doi.org/10.1017/9781009325844

H.-O. Pörtner, D. C. Roberts, M. Tignor, E. S. Poloczanska, K. Mintenbeck, A. Alegría, et al. (Eds.), *Climate change 2022: Impacts, adaptation and vulnerability. Contribution of working group II to the sixth assessment report of the Intergovernmental Panel on Climate Change* (3056 pp.). Cambridge University Press. https://doi.org/10.1017/9781009325844

Latham, J., Bower, K., Choularton, T., Coe, H., Connolly, P., Cooper, G., et al. (2012). Marine cloud brightening. *Philosophical Transactions of the Royal Society A: Mathematical, Physical & Engineering Sciences*, *370*(1974), 4217–4262. https://doi.org/10.1098/rsta.2012.0086

Leach, N. J., Jenkins, S., Nicholls, Z., Smith, C. J., Lynch, J., Cain, M., et al. (2021). FaIRv2.0.0: A generalized impulse response model for climate uncertainty and future scenario exploration. *Geoscientific Model Development*, *14*(5), 3007–3036. https://doi.org/10.5194/gmd-14-3007-2021

Liu, P. R., & Raftery, A. E. (2021). Country-based rate of emissions reductions should increase by 80% beyond nationally determined contributions to meet the 2°C target. *Communications Earth & Environment*, *2*(1), 1–10. https://doi.org/10.1038/s43247-021-00097-8

Lund, M. T., Myhre, G., & Samset, B. H. (2019). Anthropogenic aerosol forcing under the shared socioeconomic pathways. *Atmospheric Chemistry and Physics*, *19*(22), 13827–13839. https://doi.org/10.5194/acp-19-13827-2019

McCoy, D. T., Bender, F. A.-M., Grosvenor, D. P., Mohrmann, J. K., Hartmann, D. L., Wood, R., & Field, P. R. (2018). Predicting decadal trends in cloud droplet number concentration using reanalysis and satellite data. *Atmospheric Chemistry and Physics*, *18*(3), 2035–2047. https://doi.org/10.5194/acp-18-2035-2018

McCoy, I. L., Vogt, M. A., & Wood, R. (2022). Absorbing aerosol choices influences precipitation changes across future scenarios. *Geophysical Research Letters*, *49*(8), e2022GL097717. https://doi.org/10.1029/2022GL097717

Meehl, G. A., Washington, W. M., Ammann, C. M., Arblaster, J. M., Wigley, T. M. L., & Tebaldi, C. (2004). Combinations of natural and anthropogenic forcings in twentieth-century climate. *Journal of Climate*, *17*(19), 3721–3727. https://doi.org/10.1175/1520-0442(2004)017⟨3721:CONAAF⟩2.0.CO;2

Meinshausen, M., Raper, S. C. B., & Wigley, T. M. L. (2011). Emulating coupled atmosphere-ocean and carbon cycle models with a simpler model, MAGICC6—Part 1: Model description and calibration. *Atmospheric Chemistry and Physics*, *11*(4), 1417–1456. https://doi.org/10.5194/acp-11-1417-2011

Morice, C. P., Kennedy, J. J., Rayner, N. A., Winn, J. P., Hogan, E., Killick, R. E., et al. (2021). An updated assessment of near-surface temperature change from 1850: The HadCRUT5 data set. *Journal of Geophysical Research: Atmospheres*, *126*(3), e2019JD032361. https://doi.org/10.1029/2019JD032361

Murray, C. J. L., Aravkin, A. Y., Zheng, P., Abbafati, C., Abbas, K. M., Abbasi-Kangevari, M., et al. (2020). Global burden of 87 risk factors in 204 countries and territories, 1990–2019: A systematic analysis for the global burden of disease study 2019. *The Lancet*, *396*(10258), 1223–1249. https://doi.org/10.1016/S0140-6736(20)30752-2

NOAA. (2023). National centers for environmental information (NCEI): Monthly global climate report for August 2023. Retrieved from https://www.ncei.noaa.gov/access/monitoring/monthly-report/global/202308

O'Neill, B. C., Tebaldi, C., van Vuuren, D. P., Eyring, V., Friedlingstein, P., Hurtt, G., et al. (2016). The scenario model intercomparison project (ScenarioMIP) for CMIP6. *Geoscientific Model Development*, *9*(9), 3461–3482. https://doi.org/10.5194/gmd-9-3461-2016

Pendergrass, A. G., & Hartmann, D. L. (2013). The atmospheric energy constraint on global-mean precipitation change. *Journal of Climate*, *27*(2), 757–768. https://doi.org/10.1175/JCLI-D-13-00163.1

Persad, G. G., & Caldeira, K. (2018). Divergent global-scale temperature effects from identical aerosols emitted in different regions. *Nature Communications*, *9*(1), 3289. https://doi.org/10.1038/s41467-018-05838-6

Persad, G. G., Samset, B. H., & Wilcox, L. J. (2022). Aerosols must be included in climate risk assessments. *Nature*, *611*(7937), 662–664. https://doi.org/10.1038/d41586-022-03763-9

Qu, X., Hall, A., Klein, S. A., & DeAngelis, A. M. (2015). Positive tropical marine low-cloud cover feedback inferred from cloud-controlling factors. *Geophysical Research Letters*, *42*(18), 7767–7775. https://doi.org/10.1002/2015GL065627

Quaas, J., Jia, H., Smith, C., Albright, A. L., Aas, W., Bellouin, N., et al. (2022). Robust evidence for reversal of the trend in aerosol effective climate forcing. *Atmospheric Chemistry and Physics*, *22*(18), 12221–12239. https://doi.org/10.5194/acp-22-12221-2022

Quaas, J., Ming, Y., Menon, S., Takemura, T., Wang, M., Penner, J. E., et al. (2009). Aerosol indirect effects—General circulation model intercomparison and evaluation with satellite data. *Atmospheric Chemistry and Physics*, *9*(22), 8697–8717. https://doi.org/10.5194/acp-9-8697-2009

Riahi, K., van Vuuren, D. P., Kriegler, E., Edmonds, J., O'Neill, B. C., Fujimori, S., et al. (2017). The shared socioeconomic pathways and their energy, land use, and greenhouse gas emissions implications: An overview. *Global Environmental Change*, *42*, 153–168. https://doi.org/10.1016/j.gloenvcha.2016.05.009

Seinfeld, J. H., Bretherton, C., Carslaw, K. S., Coe, H., DeMott, P. J., Dunlea, E. J., et al. (2016). Improving our fundamental understanding of the role of aerosolcloud interactions in the climate system. *Proceedings of the National Academy of Sciences*, *113*(21), 5781–5790. https://doi.org/10.1073/pnas.1514043113

Sherwood, S. C., Webb, M. J., Annan, J. D., Armour, K. C., Forster, P. M., Hargreaves, J. C., et al. (2020). An assessment of Earth's climate sensitivity using multiple lines of evidence. *Reviews of Geophysics*, *58*(4), e2019RG000678. https://doi.org/10.1029/2019RG000678

Smith, C., Nicholls, Z. R. J., Armour, K., Collins, W., Forster, P., Meinshausen, M., et al. (2021). The Earth's energy budget, climate feedbacks, and climate sensitivity supplementary material. In V. Masson-Delmotte, P. Zhai, A. Pirani, S. L. Connors, C. Péan, S. Berger, et al. (Eds.), *Climate Change 2021: The Physical Science Basis. Contribution of Working Group I to the Sixth Assessment Report of the Intergovernmental Panel on Climate Change*. Retrieved from https://ipcc.ch/static/ar6/wg1

Stjern, C. W., Muri, H., Ahlm, L., Boucher, O., Cole, J. N. S., Ji, D., et al. (2018). Response to marine cloud brightening in a multi-model ensemble. *Atmospheric Chemistry and Physics*, *18*(2), 621–634. https://doi.org/10.5194/acp-18-621-2018

Taylor, K. E., Crucifix, M., Braconnot, P., Hewitt, C. D., Doutriaux, C., Broccoli, A. J., et al. (2007). Estimating shortwave radiative forcing and response in climate models. *Journal of Climate*, *20*(11), 2530–2543. https://doi.org/10.1175/JCLI4143.1

Turnock, S. T., Allen, R. J., Andrews, M., Bauer, S. E., Deushi, M., Emmons, L., et al. (2020). Historical and future changes in air pollutants from CMIP6 models. *Atmospheric Chemistry and Physics*, *20*(23), 14547–14579. https://doi.org/10.5194/acp-20-14547-2020

Twomey, S. (1977). The influence of pollution on the shortwave albedo of clouds. *Journal of the Atmospheric Sciences*, *34*(7), 1149–1152. https://doi.org/10.1175/1520-0469(1977)034⟨1149:TIOPOT⟩2.0.CO;2

Watson-Parris, D., & Smith, C. J. (2022). Large uncertainty in future warming due to aerosol forcing. *Nature Climate Change*, *12*(12), 1111–1113. https://doi.org/10.1038/s41558-022-01516-0

Wilcox, L. J., Allen, R. J., Samset, B. H., Bollasina, M. A., Griffiths, P. T., Keeble, J., et al. (2023). The regional aerosol model intercomparison project (RAMIP). *Geoscientific Model Development*, *16*(15), 4451–4479. https://doi.org/10.5194/gmd-16-4451-2023

Wood, R. (2021). Assessing the potential efficacy of marine cloud brightening for cooling Earth using a simple heuristic model. *Atmospheric Chemistry and Physics*, *21*(19), 14507–14533. https://doi.org/10.5194/acp-21-14507-2021

Zelinka, M. D. (2021). *mzelinka*. Zenodo. https://doi.org/10.5281/zenodo.5514142

Zelinka, M. D., Myers, T. A., McCoy, D. T., Po-Chedley, S., Caldwell, P. M., Ceppi, P., et al. (2020). Causes of higher climate sensitivity in CMIP6 models. *Geophysical Research Letters*, *47*(1), e2019GL085782. https://doi.org/10.1029/2019GL085782

Zelinka, M. D., Smith, C. J., Qin, Y., & Taylor, K. E. (2023). Comparison of methods to estimate aerosol effective radiative forcings in climate models. *Atmospheric Chemistry and Physics*, *23*(15), 8879–8898. https://doi.org/10.5194/acp-23-8879-2023

Erratum

The originally published version of this article contained typographical errors. In the third sentence of the first paragraph of Section 3, "S20" should be changed to "S21," and the subsequent mentions of "S20" should be changed to "S21." The errors have been corrected, and this may be considered the authoritative version of record.